Modeling of Anisotropy in the Lithosphere and Asthenosphere for Real Earth Cases: A Critical Assessment of the Impact on SKS Measurements

Gaelle Lamarque, Nicola Piana agostinetti

JGR Solid Earth

RESEARCH ARTICLE
10.1029/2019JB018978

Key Points:
- We analyze the effects of realistic Earth's lithospheric structures on SKS splitting parameters
- Highly anisotropic crustal materials can explain 40% of the SKS time delay
- In realistic cases, the observed average SKS splitting direction does not always represent the asthenospheric flow direction

Supporting Information:
- Supporting Information S1

Correspondence to:
N. Piana Agostinetti,
nicola.piana.agostinetti@univie.ac.at

Citation:
Lamarque, G., & Piana Agostinetti, N. (2020). Modeling of anisotropy in the lithosphere and asthenosphere for real Earth cases: A critical assessment of the impact on SKS measurements. *Journal of Geophysical Research: Solid Earth*, *125*, e2019JB018978. https://doi.org/10.1029/2019JB018978

Received 31 OCT 2019
Accepted 16 MAY 2020
Accepted article online 21 MAY 2020

Modeling of Anisotropy in the Lithosphere and Asthenosphere for Real Earth Cases: A Critical Assessment of the Impact on SKS Measurements

Gaelle Lamarque[1,2] and Nicola Piana Agostinetti[3,4]

[1]Laboratoire Geosciences Ocean, UMR6538, IUEM, UBO, Plouzané, France, [2]Ifremer, Geosciences Marines, Centre de Brest, Plouzané, France, [3]Department of Geodynamics and Sedimentology, Faculty of Earth Sciences, Geography and Astronomy, University of Vienna, Vienna, Austria, [4]Centro Nazionale Terremoti, Istituto Nazionale di Geofisica e Vulcanologia, Rome, Italy

Abstract We investigate effects of realistic Earth's lithospheric structures on measurements of SKS seismic waves birefringence, which could be perturbed by different factors. We present SKS measurements recorded in four different tectonic settings. For each case, a realistic lithospheric structure is assumed and synthetic SKS splitting measurements are compared with the field observations. Our results show that (a) in a simple case, where anisotropy is aligned in both the lithospheric mantle and the asthenosphere, the SKS measurements can be safely interpreted as dominantly related to asthenospheric mantle flow; (b) in case of multilayer anisotropy in the lithospheric mantle, SKS measurement can correspond to a combination of the different fast-axis orientations and intensities of the anisotropic layers, dominated by the layer with stronger anisotropy; (c) across orogens, where highly anisotropic (≥10%) crustal sections are present, a relevant percent (30–40%) of SKS measurement can be explained by crustal contributions, with additional challenge related to the different direction of retrieved and expected symmetry axis; and finally, (d) in subduction zones, even in the absence of mantle corner flow, subducted crust materials can interplay with the overriding plate to generate an interpretable SKS observation. We conclude that complex crustal and/or lithospheric anisotropy can lead to erroneous SKS splitting parameters interpretations in terms of mantle deformations. We show in particular that complex crustal anisotropy can produce both important time delay and back azimuthal pattern. We also confirm that SKS splitting parameters do not allow to identify the presence of more than two anisotropic layers in the mantle.

1. Introduction

Measuring seismic anisotropy within the Earth is essential as it constitutes a proxy for inferring upper mantle deformation related to mantle flow that develops preferred orientations of the minerals in response to tectonic strain (Mainprice et al., 2000; Nicolas & Christensen, 2013; Silver et al., 1999). The most used and longest-standing method to detect anisotropy beneath a seismic station is the measurement of teleseismic core-refracted SKS, SKKS, PKS, and PKKS (hereinafter referred to as XKS) wave splitting on two horizontal recordings. This method consists on measuring the direction of fast polarization (φ) and the delay time (δt) between the two fast- and slow- polarized shear waves generated by the presence of anisotropic material. This technique allows an integrative measurement which estimates the average φ and δt along the entire XKS raypath. The nearly vertical propagation of XKS waves within the lithosphere and the asthenosphere beneath the seismic station provides high lateral but poor vertical resolution on the measurement of anisotropy.

This lack of depth-dependent resolution related to the presence of anisotropy at depth can result in misinterpretation regarding mantle deformation in several cases and, consequently, can lead to erroneous geodynamical implications. For example, discrimination between crustal and mantle anisotropy is essential to infer deformation processes in orogenic belts or continental rifting (Gueydan et al., 2008; Meissner et al., 2002). Questions regarding (de)coupling at the Moho boundary and implications for lithospheric deformations remain highly debated (Brun, 2002; Vauchez et al., 1998). Latifi et al. (2018) show with synthetic examples that even for simplistic models with only one moderate to weak anisotropic layer with horizontal axis of symmetry, the crust can have significant impact on the XKS splitting parameters. It is thus important to

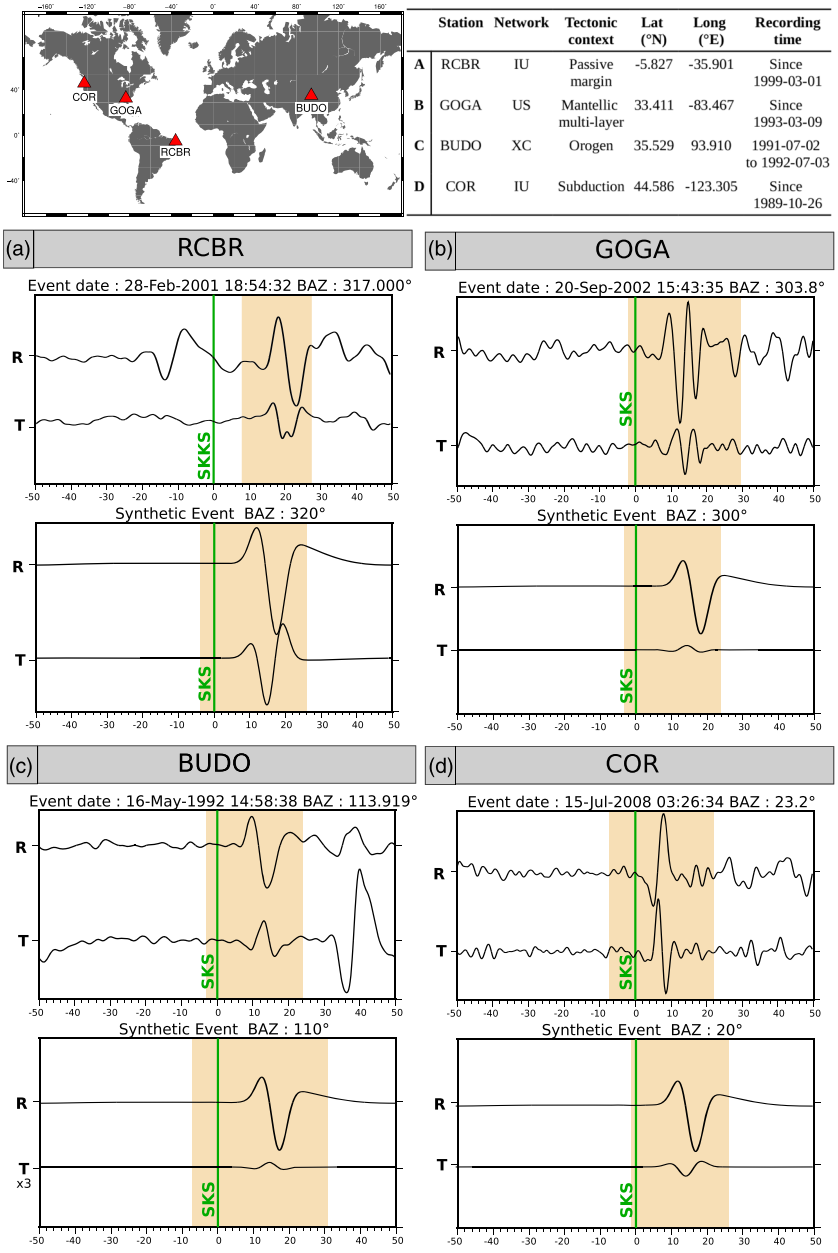

	Station	Network	Tectonic context	Lat (°N)	Long (°E)	Recording time
A	RCBR	IU	Passive margin	-5.827	-35.901	Since 1999-03-01
B	GOGA	US	Mantellic multi-layer	33.411	-83.467	Since 1993-03-09
C	BUDO	XC	Orogen	35.529	93.910	1991-07-02 to 1992-07-03
D	COR	IU	Subduction	44.586	-123.305	Since 1989-10-26

Figure 1. Localization of selected stations and examples of observed and synthetic XKS phases at each station. The green line represents the arrival time as predicted by automatic traveltime calculation. The yellow window corresponds to the manually selected window for XKS phase analyses. Note that amplitudes of the synthetic transverse components are multiplied by 3 for station BUDO.

understand the effect of crustal anisotropy for more realistic crustal models including several anisotropic layers with both horizontal and plunging axis of symmetry. In fact, XKS measurements are highly sensitive to anisotropic media with horizontal axis of symmetry, but they could be difficult to interpret in a region with plunging axis of symmetry (such as a subduction zone), unless combining them with other independent seismic data (Levin et al., 2007; Plomerová et al., 1996; Yuan & Levin, 2014). Finally, Silver and Savage (1994) and Rümpker and Silver (1998) highlighted that, in the case of two horizontal anisotropic layers, the resultingtime delay recorded at the surface can be either decreased or increased and azimuthal variations on the polarization direction of the fast wave can be observed (or not) depending on the relative direction of the two layers. All these results question the complexity of interpreting XKS measurements in regions where several (more than two) anisotropic layers occur.

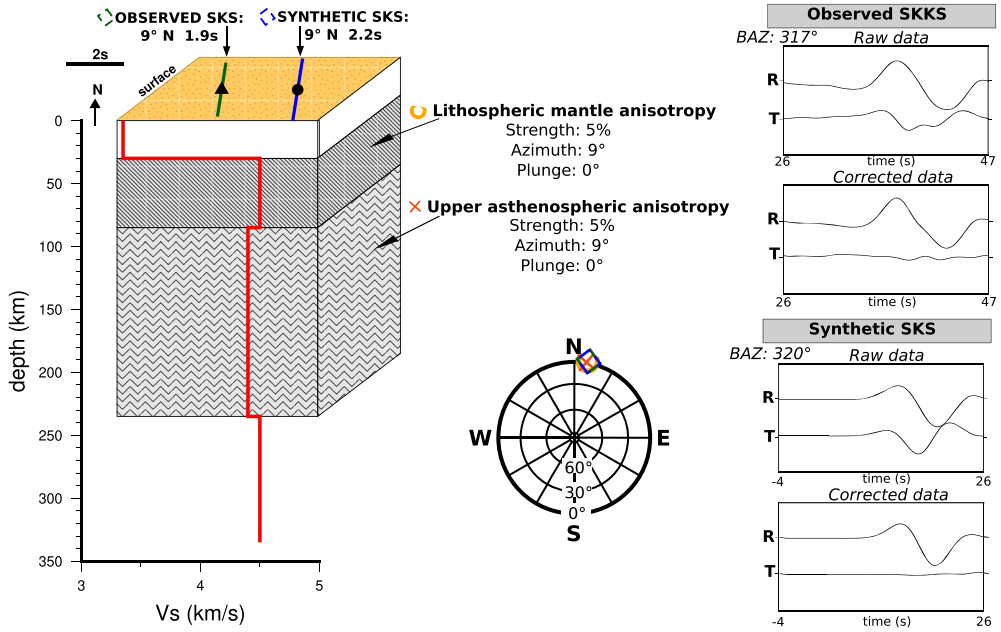

Figure 2. Summary of velocity model and splitting measurements for both real and synthetic data at station RCBR. The *S* wave velocity model is plotted in red with anisotropic layers drawn in gray. Synthetic splitting parameters obtained for this velocity model are represented by the blue line and real data by the green line. The length of the segments represent the amplitude of the delay time, and their direction the azimuth of the fast split shear wave. The caneva summarizes the input anisotropic orientations for synthetic computations (points and crosses), as well as the mean anisotropy orientations (diamonds) after analyses of observed (green diamond) and synthetic (blue diamond) data. Right panels represent examples of raw and corrected data for both observed and synthetic XKS phases with similar back azimuth as presented in Figure 1. The time window presented corresponds to the yellow window in Figure 1.

The aim of this study is to investigate the effect of complex crustal and/or lithospheric structures on XKS splittingparameters considering "realistic cases." For that purpose, we select four representative tectonic environments sampled by four seismic stations, where velocity models and anisotropic layers are well defined within the lithosphere from geo-observables other than XKS, in order to evaluate the impact of such features on XKS measurements. In particular, we focus our study on (1) a divergent passive margin region, where coherent anisotropic layers within the lithospheric mantle and the asthenosphere (station RCBR, Brazil) are expected; (2) a region where subsequent stages of deformation generated multiple anisotropic layers within the mantle (station GOGA, eastern United States); (3) a collisonal orogen, where different geo-observables pointed out a complex crustal structure including multiple anisotropic layers with both horizontal and dipping axis of symmetry (station BUDO, Tibet); and (4) a subduction zone where anisotropic lithosphereis dominated by several anisotropic layers with a steeply dipping axis of symmetry (station COR, western United States). For each region, we compute an observed XKS data set (and/or we collected results from previous XKS studies, if available) to use as a benchmark for our synthetic SKS measurements. Then, we compose an anisotropic model of the lithosphere based on literature, and we perform forward simulation of SKS wave through such model, to obtain a synthetic SKS data set of SKS splitting measurements. The goal of our modeling approach is not to precisely fit the data but to compute synthetic SKS out of previously established anisotropic models (i.e., without trying to modify the single model for improving the fit to SKS observations). Additionally, for having a uniform approach, where a single study reporting the entire lithosphere and asthenosphere anisotropic model is not existent, we compose the model integrating more than one source of constraints on anisotropic structure. Comparison between observed XKS and synthetic SKS data set allows us to discuss the effect of simple-to-complex lithospheric anisotropy on such observable.

2. Data and Method

For this study we selected four seismic stations, which are listed together with their coordinates, locations, networks, and recording times in Figure 1. In order to evaluate the impact of complex structures to XKS splitting parameters, we performed synthetic SKS waves propagating through crustal or lithospheric velocity models defined from previous studies (see the following sections for details about velocity models). Such

studies generally involved other seismic observables (e.g., receiver function and/or surface waves) and exclude XKS measurements, for defining the anisotropic layering. Synthetic SKS waves are obtained from Frederiksen and Bostock (2000) software. We then measured splitting parameters from synthetic SKS waves and compare them to real XKS data at the corresponding station. Note that synthetics data were computed for a set of back azimuths which correspond to the real back azimuthal coverage recorded at the station for XKS measurements.

Both synthetics and real data splitting measurements were performed using SplitRacer software (Reiss & Rümpker, 2017). For real data, we selected events with epicentral distance between 85° and 140° from the seismic station and with magnitude higher than or equal to 6. At station BUDO, which recorded only 1 year data, we extended our analysis to earthquakes with magnitude higher than or equal to 5. Single splitting analysis is based on the minimum eigenvalue method (Silver & Chan, 1991), which performs a grid search over φ and δt that best linearizes the particle motion and thus best corrects the anisotropy within the selected measurement window. Data were filtered between 4 and 50 s, and signals with signal-to-noise ratio below 2.5 were automatically discarded. Measurements are repeated for a number of time windows to enable statistical error analysis. We determined the quality (good, fair, poor, or null) of each individual measurement by applying manual evaluation according to a set of criteria defined as the signal-to-noise ratio of the initial waveform(only for real data), the correlation between the fast and slow shear waves, the linearity of the particle motion in the horizontal plane after correction, and of the size of the 95% confidence area (Barruol et al., 1997).

The average values of splitting parameters φ and δt per station are obtained from SplitRacer software, which calculates an average layer model assuming an average period of 10 s for the phases with standard deviations for the splitting parameters of 20° and 1 s. This calculation includes "good," "fair," and "null" quality measurements but do not take into account "poor" quality measurements.

3. A Simple Case: Multiple Anisotropic Layers in the Lithosphere, With Subhorizontal and Parallel Symmetry Axes

At station RCBR we study the case where only horizontal anisotropic layers with parallel fast axis of symmetry occur. We use this simple case as a standard in order to validate the methodology. Left panel of Figure 2 represents the velocity model used to generate SKS synthetics waves. The model has been compiled using the results from Bastow et al. (2011), Heit et al. (2007), Liu et al. (2019), and Lamarque and Juliá (2019), where the authors analyzed fast-polarization direction from SKS splitting analysis, Moho and lithosphere-asthenosphere boundary depths from *S* wave receiver functions, intensity of anisotropy from EBSD measurements, and direction of anisotropy within the lithospheric mantle from harmonic stripping of *P* wave receiver functions, respectively, for making inferences on the lithospheric seismic structure. Details for this model are presented in Table A1. Average splitting parameters for real data are reported in Figure 2, appendix Table B1, and section C.1). Both Assumpção et al. (2011) and this study retrieved similar fast-polarization direction but different time delay. The two studies performed similar calculation to retrieve the splitting parameters by using both Silver and Chan (1991) algorithm. Different values for δt must be related to manual selection and quality classification of events. We choose to use time delay computed by Assumpção et al. (2011) because (i) uncertainties are much more lower in his study, (ii) 1.9 s is much more realistic than 3 s in passive margin context, and (iii) 1.9 s is included in the 95% confidence level in our study, and it is thus as probable as 3 s. Coherent fast-polarization directions in the two anisotropic layers is proposed to explain the large time delay measured from real data (Assumpção et al., 2011). Results from synthetic SKS waves provide splitting parameters $\varphi = 9°\text{N}$ and $\delta t = 2.2$ s which explains well the real measurements done at this station. In that case, time delays produced within each individual layer are summed up to finally give the large time delay measured at the surface. This sum is only possible in the case of parallel fast axis of symmetry in the two layers.

4. Getting Complex: Multiple Anisotropic Layers in the Lithosphere With Differently Oriented Symmetry Axis

GOGA station is located in the eastern Appalachian region in the United States, where three anisotropic layers with different fabrics have been identified by surface wave tomography (Deschamps et al., 2008).

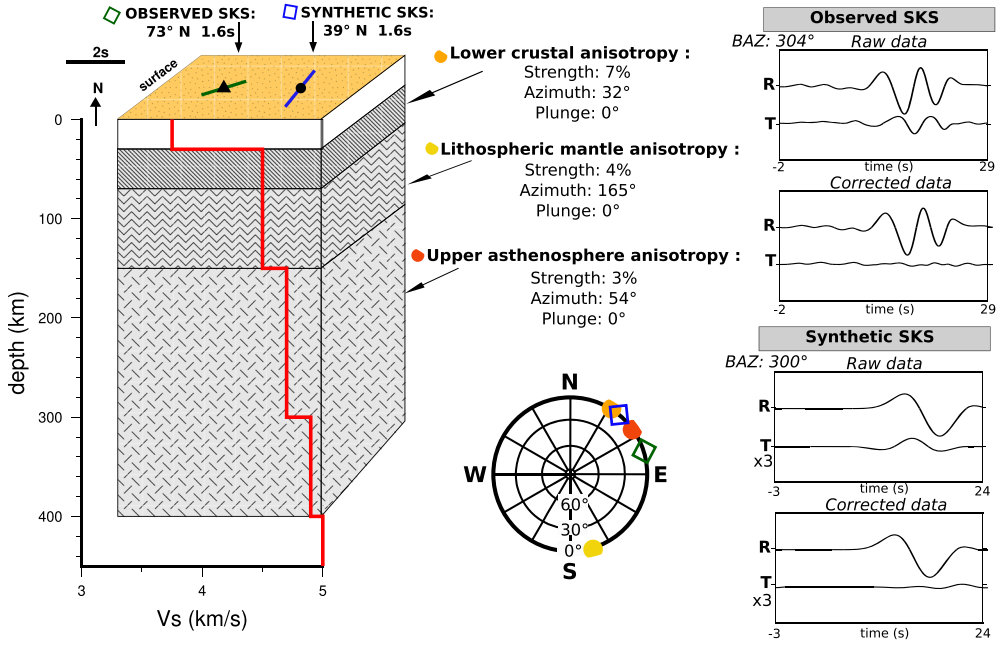

Figure 3. Same as Figure 2 but for station GOGA. Velocity model parameters are based on Deschamps et al. (2008). Amplitudes of the synthetic transverse components (raw and corrected data) are multiplied by 3.

These authors inverted phase velocity maps and pairs of selected measured dispersion curves, highlighting the presence of two anisotropic layers within the lithosphere (30–70 and 70–150 km depths) and one anisotropic layer within the asthenosphere (deeper than 150 km) with fast axis of hexagonal symmetry from top to bottom oriented 32°N, 165°N, and 54° N, respectively (see Figures 3 and 5 of Deschamps et al., 2008). All these layers are supposed to have horizontal axis of symmetry. Figure 3 represents the velocity model used to generate SKS synthetic waves, which is also presented in detail in Table A2. Average splitting parameters for real and synthetic data are reported in Figure 3, appendix Table B1, and section C.2). Synthetic SKS provide results with [R1.11] different trend but similar time delay to the observed XKS parameters at the surface. XKS splitting at station GOGA has been analyzed many times, from different research groups (Barruol et al., 1997; Liu, 2009; Long et al., 2010; Yang et al., 2017). In some studies, the authors only found null measurements (Long et al., 2010), while others were able to compute splitting parameters from SKS waves (Barruol et al., 1997; Yang et al., 2017). This discrepancy was already discussed in Yang et al. (2017). From our side, we computed 92 good/average SKS splitting measurements that have been used in our study and which are consistent with results from Yang et al. (2017). In Figure 4, splitting parameters for both observed (gray crosses) and synthetic (blue circles) data are represented in functions of back azimuth. Red crosses correspond to the average value per back azimuth for observed data, which are calculated by a simple average formula taking only into account the values (not the standard deviation) of splitting parameters from "good" and "average" events (not null measurements). The red (observed data) and blue (synthetic data) lines correspond to the splitting parameters of the average layer as calculated by Splitracer software. This calculation takes into account "good," "fair," and "null" measurements. We notice that both average observed (red crosses) and synthetic (blue circles) data display similar back azimuthal patterns for both fast-polarization direction (Φ) and time delay (δt). By inverting the synthetic results, we found that a two-layer model composed of (i) a top layer with splitting parameters 30°N and 1.6 s and (ii) a bottom layer with splitting parameters 100°N and 0.4 s perfectly fits the data. Splitting results for such model are presented in green in Figure 4. The fact that a two-layer model fits our synthetic results made from a three-layer model indicates that inversion of SKS waves cannot identify the presence of more than two anisotropic layers. We also notice that the average values of the φ direction for the synthetic data (blue line in Figure 4) is closely related to the most anisotropic layer (the top one in our case). Moreover, results from synthetics perfectly fit

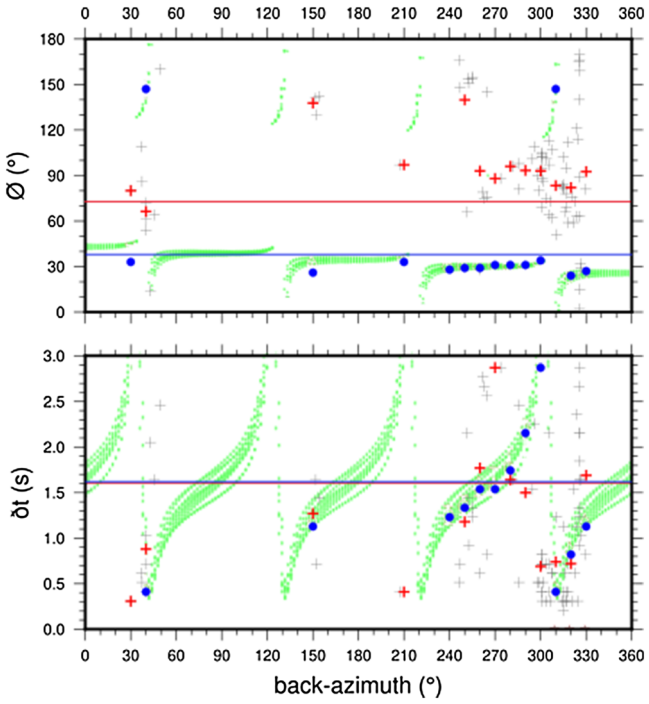

Figure 4. Results at station GOGA for synthetics SKS (blue circles) and XKS observed data (gray crosses) splitting parameters in functions of back azimuth. Red crosses represent the average value for observed data for a 10° back azimuth interval. Upper panel represents the polarization direction of the fast *S* wave, and lower panel corresponds to the time delay between the fast and the slow *S* waves. As an indication, splitting parameters of the average layer model for synthetics (blue line) and observed data (red line) are represented. The light green circles represent the best model after inversion of the synthetics SKS.

observed time delay and are shifted by ~40° for fast-polarization direction. We assume that this shift could be related to crustal anisotropy, which we investigate in the two following examples.

5. Complex Crustal Anisotropy Including Dipping Symmetry Axis

5.1. With Horizontal Fast Axis of Symmetry Into the Mantle

In order to study the influence of complex shallow crustal anisotropy (0–20 km depth range) on XKS splitting, we choose BUDO station in Tibet. The selection of this station has been made by the availability of a detailed crustal model which is constrained by four different studies (see below) which mostly agree on the velocity and anisotropy structure of the crust beneath this station. Figure 5 represents the velocity model used to generate SKS synthetics waves, which is also presented in detail in Table A3. This model is made by summing crustal structure extracted from receiver functions and mantle anisotropy inferred from surface waves. Anisotropic structure within the crust is based on Licciardi and Piana Agostinetti's (2016) work, which matches pretty well previous studies on crustal anisotropic layers at the same station (Frederiksen et al., 2003; Sherrington et al., 2004; Vergne et al., 2003). Main outlines of this model are the presence of two anisotropic layers with opposite axis of symmetry directions ($\varphi = 19$ and -160 for top and bottom layers, respectively). Moreover, the top anisotropic layer has a horizontal axis of symmetry, whereas the bottom one is characterized by 55° plunging axis of symmetry. Anisotropy within the mantle is based on surface waves analysis of Pandey et al. (2015), who identified four layers with horizontal fast axis of symmetry oriented 125°N, 0°N, 35°N, and 90°N, respectively. Average splitting parameters for real and synthetic data are reported in Figure 5, appendix Table B1, and section C.3. Average polarization direction for synthetics XKS waves (dark blue in Figure 5) propagating through this model fits the observed data. We also notice that synthetic SKS waves propagating only through the crustal model produce an apparent fast-polarization direction which is also subparallel to the observed XKS waves. This observation indicates that the crust significantly contributes to the observed SKS splitting. In fact, synthetic SKS waves for the crustal contribution display time delay δt equal to 0.8 s, which accounts for 33% (or 44%) of the time delay recording at the surface, $\delta t = 2$ s, this study (or $\delta t = 2.4$ s McNamara et al., 1994). Moreover, it is worth noticing that the apparent phi direction computed from synthetic data using only crustal anisotropic layers is almost 90° from the direction of the symmetry axis of such two layers. This fact is probably due to the concurrent effects of plunging axis (lower crustal layer) and change from anisotropy with slow (due to aligned cracks) to fast axis of symmetry (generated by the alignment of elongated mineral grains, Sherrington et al., 2004). Summing/subtracting *t* delays in case of complex anisotropy could give misleading insights.

5.2. With Plunging Subslab Anisotropy Into the Mantle

Corvalis (COR) station is located above the Cascadia subduction zone. Park et al. (2004) have shown that no corner mantle flow is observed beneath that station because they identified a low-velocity (Vp = 6.0 km/s) layer made up of materials with strong slow axis of symmetry (−7%) which is unlikely to represent olivine material. The proposed model includes the superposition of a complex continental lithosphere above the plunging oceanic plate and the subslab mantle, including methamorphosed mafic crust (Piana Agostinetti & Miller, 2014). Following the receiver function analysis presented in Park et al. (2004), the shallow structure (<50 km depth) is characterized by the presence of four crustal anisotropic layers with varying anisotropy intensity and axis of symmetry direction and plunging. The slab and subslab directions are taken from Roth et al. (2008), which are both deduced from XKS data, and slab geometry from Fowler (1990). Figure 6 represents the velocity model used to generate SKS synthetics waves, which is also presented in

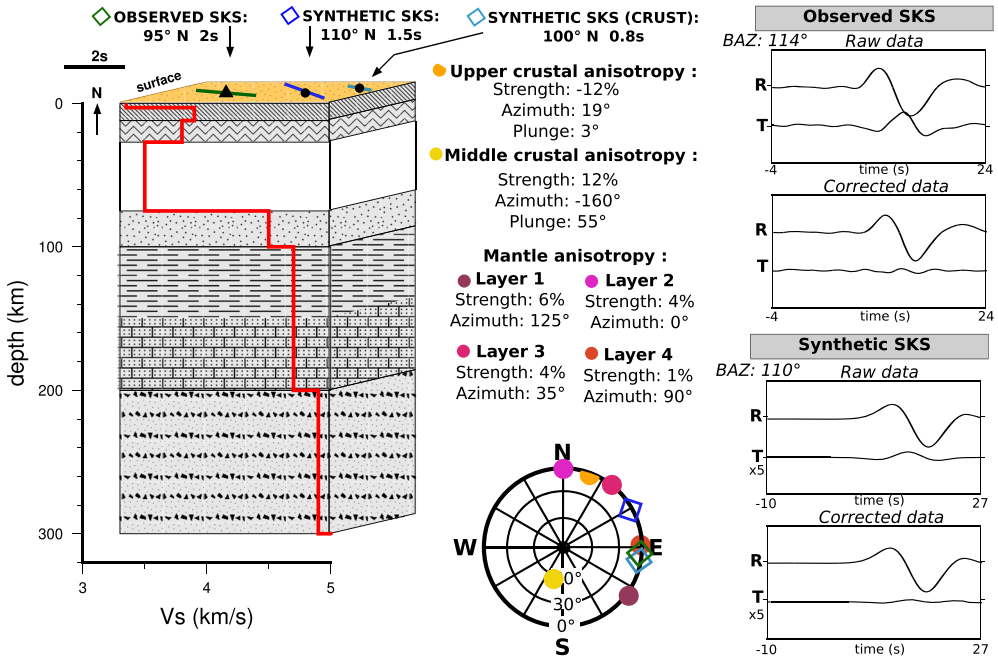

Figure 5. Same as Figure 2 but for station BUDO. Velocity model parameters are based on Licciardi and Piana Agostinetti (2016). Amplitudes of the synthetic transverse components (raw and corrected data) are multiplied by 5.

detail in Table A4. Average splitting parameters for real and synthetic data are reported in Figure 6, appendix Table B1, and section C.4). The average XKS splitting parameter measured at the surface is ENE-SWS, in agreement with previous studies (Eakin et al., 2010; Martin-Shortet al., 2015).

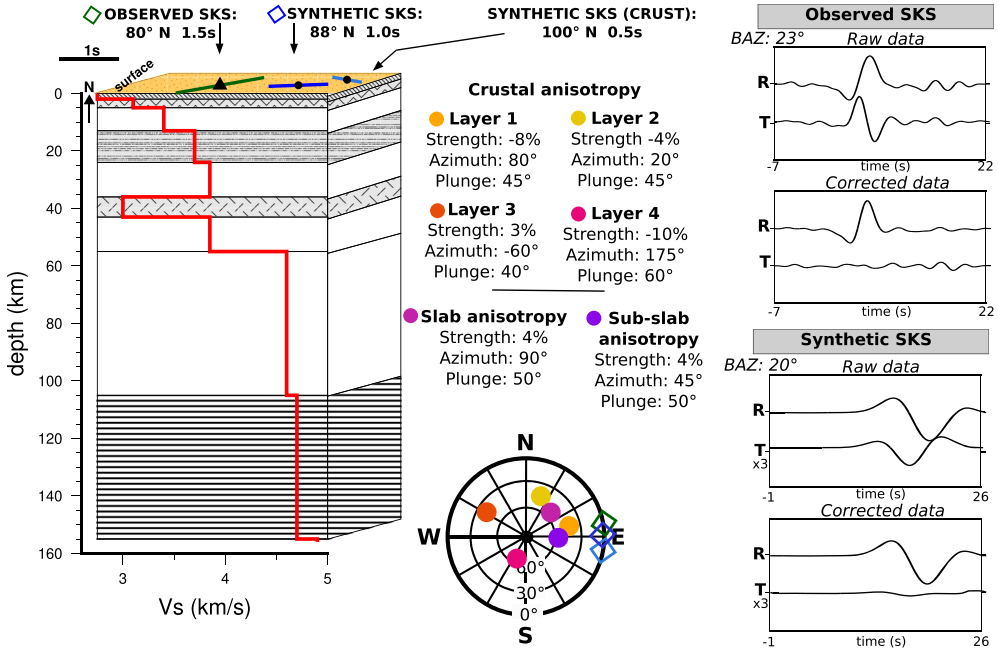

Figure 6. Same as Figure 2 but for station COR. Velocity model parameters are based on Park et al. (2004). Amplitudes of the synthetic transverse components (raw and corrected data) are multiplied by 3.

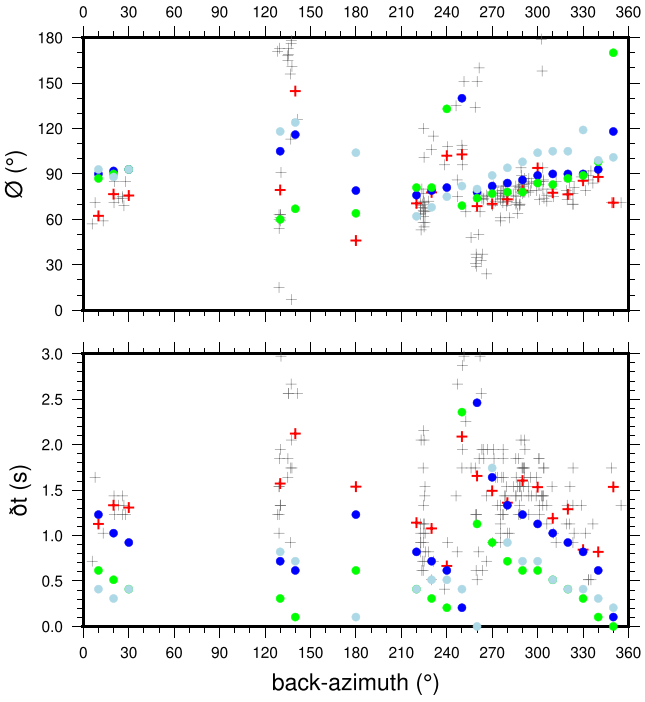

Figure 7. Results at station COR for observed (gray crosses), mean value per 10° back azimuth intervals (red crosses), synthetics for the complete model presented in Figure 6 (dark blue circles), synthetics for the crust only (light blue circles), and synthetics for the slab and subslab only (green circles) XKS splitting parameters in functions of back azimuth. Upper panel represents the polarization direction of the fast *S* wave, and lower panel corresponds to the time delay between the fast and the slow *S* waves.

Once again, as for station BUDO, the average polarization direction for synthetic SKS waves propagating through the entire model seems, interestingly, not related with any direction (even not to the subslab mantle flow), but it is relatively aligned to the polarization direction measured at the surface. Moreover, by modeling SKS waves propagating only through the upper plate, we make similar observations that the apparent polarization direction ($\varphi = 100°$N) is relatively aligned to the polarization direction measured at the surface. The concordance between these three results highlights the contribution of the upper plate shallow structure to the XKS splitting measured at the surface, which accounts for 33% of the total δt (i.e., 0.5 s estimated for the synthetics and 1.5 s measured at the surface).

The localization and long-time recording at this station allow us to observe the dependency of splitting parameters on the back azimuth of the incoming XKS wave. Figure 7 represents splitting parameters in functions of back azimuth for (i) synthetic waves for the entire model (dark blue circles), (ii) synthetic waves for the upper anisotropic lithosphere only (light blue circles), (synthetic waves for the slab and subslab only (green circles), and (iv) recorded waves at the surface (gray and red crosses). This figure highlights that complex anisotropic lithosphere can produce back azimuthal patterns on splitting parameters φ and δt. We also notice that synthetic and measured splitting parameters display similar patterns, including for synthetics produced only from the upper lithosphere model. This observation suggests that at COR station the back azimuthal pattern can be explained by the complex anisotropic lithosphere depicted in Park et al. (2004) and that the contribution of deeper anisotropic material (slab and subslab) do not contribute to the relevant back azimuthal pattern. Moreover, apparent splitting direction at the surface is absolutely not related to the subslab fast axis of symmetry but results from a combination of complex crustal and mantle anisotropy.

6. Potential Pitfalls in XKS Measurement Interpretations

In this study, we focus on pitfalls related to incorrect parametrization of the Earth (i.e., not considering crustal anisotropy), dipping symmetry axis for anisotropic layers, and/or the presence of more that two anisotropic layers. A broader description of potential pitfalls in real data can be also found in Vecsey et al. (2008). The examples presented in this study highlight several potential pitfalls while interpreting XKS measurements. These pitfalls would come as no surprise to most shear wave splitting analysts as these are well-known issues of SKS splitting interpretation and they are well established in literature. Our examples move the discussion a step forward to a broader audience of geoscientists because interpretations of SKS splitting measurements in terms of mantle flow are widespread in geophysical literature, but those pitfalls are not always carefully considered as we show they should be.

The analysis for obtaining XKS measurements is actually robust because it does not need heavy processing, but the near-vertical geometry of their raypath prohibits any vertical resolution. We show with station RCBR (northeast Brazil—divergent passive margin) that in a simple case with one or several mantellic anisotropic layer(s) with parallel fast axis of symmetry (and no or negligible crustal anisotropy), it is relatively straightforward to interpret XKS measurements. In that case, the measured fast axis of symmetry is directly related to fast axis of symmetry at depth, and the entire time delay can be attributed to mantle deformation (both lithospheric and asthenospheirc mantle).

At station GOGA, we investigate the effect of an anisotropic structure that comprises more than two horizontal anisotropic layers within the mantle, with nonparallel symmetry axis. First, we notice that synthetic SKS waves computed with this velocity model do not fully reproduce XKS splitting parameters observed at

the surface. Such observation argues in favor of joint inversion/interpretation of several seismic data set in order to propose a comprehensive velocity model that explains at best independent data (Babuška et al., 1993, 2008; Plomerová et al., 1996; Plomerová & Babuška, 2010; Romanowicz & Yuan, 2012). The back azimuthal variations of synthetic SKS parameters is very limited and could be missed in the presence of back azimuthal gaps larger than 90° (as in the case of GOGA station). Our synthetic test using a realistic multilayer structure of the upper mantle indicates that by looking at XKS splitting parameters only one could miss information about the presence of several anisotropic layers (Savage, 1999). Once again, the use of others methods such as surface waves tomography or receiver functions is fundamental to constrain the upper structure along the raypath of the XKS waves and, by coupling these models to XKS data, better estimate depth-dependent anisotropy within the lithosphere and the asthenosphere.

Along the Himalayan collisional orogen, we show that in the presence of complex crustal anisotropy, expected in most of the tectonically active area worldwide (here, station BUDO, but also at station COR above the Cascadia subduction zone), the crust can account for a large (up to 30–40%) amount of the observed time delay. In these two cases, the shallow Earth structure (<50 km) is composed of several anisotropic layers with dipping fast or slow axis of symmetry directions, not oriented parallel to each other. But the resulting apparent SKS wave is subparallel to the observed XKS. We can thus conclude that here, the time delay must be 30–40% reduced in order to interpret the XKS measurements in terms of mantle deformation.

Contrary to what happens at station GOGA, our analysis of station COR station highlighted that complex crustal anisotropy can produce back azimuthal pattern which could be misinterpreted in terms of multiple anisotropic layers within the mantle. In this specific example, we suggest that anisotropy within the subducted Juan de Fuca mantle could simply increase the observed delay time, without affecting the back azimuthal pattern related to crustal anisotropy. Thus, it is necessary to estimate velocity and anisotropy models for the crust (and the entire lithosphere) in order to evaluate the impact of shallow structures on splitting parameters.

7. Conclusions

By studying four examples of anisotropy complexity beneath selected stations, we highlight potential pitfalls in XKS splitting parameters interpretations.

1. We show that the crust can account for a large (up to 40%) amount of the recorded time delay in different tectonic systems (orogenesis and subduction zone).
2. Moreover, complex anisotropic crustal structures can produce XKS back azimuthal pattern, which needs to be identified before interpreting XKS measurements in terms of mantle structure constituted by multiple layers.
3. In case of multilayer anisotropic mantle, with horizontal and/or dipping symmetry axis, the observed average SKS splitting direction, phi, is not always representative of the direction of flow in the asthenospheric mantle.

To avoid such interpretation bias, XKS measurements need to be carefully coupled with other seismological studies (e.g., surface waves, receiver function, and local *S* wave splitting). Our results suggest that, in most of the tectonically active areas, the joint use of these methods should be "a must" for determining a fine-scaled velocity and anisotropy model for the upper part of the XKS raypath in order to correctly input such information for geodynamic modeling.

Appendix A: Velocity Models

Velocity models are defined by a superposition of layers with a thickness, density, *P* wave velocity, *S* wave velocity, intensity of *P* wave anisotropy, intensity of *S* wave anisotropy, and direction and plunge of *P* and *S* waves anisotropy. The velocity models are detailed for RCBR station in Table A1, for GOGA in Table A2, for BUDO in Table A3, and for COR in Table A4.

Table A1
Velocity Model for Station RCBR

Thickness (km)	Density (kg/cm^3)	Vp (km/s)	Vs (km/s)	AVp (%)	AVs (%)	[R2.4] direction (°N)	Plunge (°)
30	2.6	5.8	3.35	0	0	0	0
55	3.3	8.1	4.5	5	5	9	0
150	3.3	8.0	4.4	5	5	9	0
1	3.3	8.1	4.5	0	0	0	0

Note. From right to left are represented the thickness of the layer, density, velocity of *P* wave, velocity of *S* wave, anisotropy of *P* wave, anisotropy of *S* wave, [R2.4] direction of the fast axis of symmetry, and plunge of the fast axis of symmetry.

Table A2
Same as Table A1 but for Station GOGA

Thickness (km)	Density (kg/cm^3)	Vp (km/s)	Vs (km/s)	AVp (%)	AVs (%)	[R2.4] direction (° N)	Plunge (°)
30	2.7	6.0	3.75	0	0	0	0
40	3.3	8.1	4.5	7	7	32	0
80	3.3	8.1	4.5	4	4	165	0
150	3.3	8.5	4.7	3	3	54	0
100	3.3	8.8	4.9	2	2	54	0
1	3.3	9.0	5.0	0	0	0	0

Table A3
Same as Table A1 but for Station BUDO

Thickness (km)	Density (kg/cm^3)	Vp (km/s)	Vs (km/s)	AVp (%)	AVs (%)	[R2.4] direction (° N)	Plunge (°)
0.001	2.6	5.8	3.35	0	0	0	0
3	2.6	5.8	3.35	−12	−12	19	3
9	2.6	6.7	3.9	−12	−12	19	3
15	2.6	6.6	3.8	12	12	−160	55
48	2.6	6.0	3.5	0	0	0	0
25	3.3	8.1	4.5	6	6	125	0
50	3.3	8.5	4.7	4	4	0	0
50	3.3	8.5	4.7	4	4	35	0
100	3.3	8.8	4.9	1	1	90	0
1	3.3	8.1	4.5	0	0	0	0

Table A4
Same as Table A1 but for Station COR

Thickness (km)	Density (kg/cm^3)	Vp (km/s)	Vs (km/s)	AVp (%)	AVs (%)	[R2.4] direction (° N)	Plunge (°)
0.001	2.6	4.6	2.75	0	0	0	0
2	2.6	4.6	2.75	−8	−8	80	45
3	2.6	5.4	3.1	−8	−8	20	45
8	2.6	6.1	3.4	0	0	0	0
11	2.6	6.7	3.7	3	3	300	40
12	2.6	7.1	3.85	0	0	0	0
7	2.6	6.4	3.0	−10	−10	175	60
12	2.6	7.1	3.85	0	0	0	0
50	3.3	8.1	4.6	4	4	90	50
50	3.3	8.5	4.7	4	4	45	50
1	3.3	8.1	4.6	0	0	0	0

Appendix B: Average Layer Splitting Measurements

Average of both observed and modeled splitting parameter for each station are summarized in Table B1.

Table B1
Summary of Average Layer Splitting Parameters Obtained From This Study

		Average observed		Average synthetics	
Station	Network	φ (°)	δt (s)	φ (°)	δt (s)
RCBR	IU	9	3	9	2.2
GOGA	US	73	1.6	39	1.6
BUDO	XC	95	2	110	1.5
COR	IU	80	1.5	88	1.0

Note. Both observed and synthetics results are presented.

Appendix C: Single Splitting Measurements

Every individual measurement for observed SKS splitting parameters are presented in sections C1 for station RCBR, C2 for station GOGA, C3 for station BUDO, and C4 for station COR.

C1. Station RCBR

This is a summary of individual splitting measurements results for station RCBR. From right to left are presented the date, time, phase, back azimuth, sensor correction, phi, dt, phi err min, phi err max, dt err min, dt err max, quality, and confidence level. Note that only events with "good," "fair," and "null measurements" are presented ("poor" quality events are excluded).

C2. Station GOGA

Same as section C1 but for station GOGA.

C3. Station BUDO

Same as section C1 but for station BUDO.

C4. Station COR

Same as section C1 but for station COR.

Data Availability Statement

Data used for this study are available from IRIS data center with FDSN network code IU (stations RCBR and COR—ASL/USGS, 1988), US (station GOGA—ASL/USGS, 1988), and XC (station BUDO—Owens & Wu, 1991).

Acknowledgments

We used the open-source programs SAC (Goldstein & Snoke, 2005), GMT 5 (Wessel et al., 2013), SplitRacer (Reiss & Rümpker, 2017), and Raysum (Frederiksen & Bostock, 2000) to analyze and process data, to compute synthetics, and to produce figures. The work of G. L. was supported by ISblue project, Interdisciplinary graduate school for the blue planet (ANR-17-EURE-0015) and cofunded by a grant from the French Government under the program "Investissements d'Avenir." N. P. A.'s research is funded by Austrian Science Fund (FWF) under Grant Number M2218-N29.

References

ASL/USGS (1988). Global Seismograph Network-IRIS/USGS. International Federation of Digital Seismograph Networks. Dataset/Seismic Network. https://doi.org/10.7914/SN/IU

Assumpção, M., Guarido, M., Lee, S. v. d., & Dourado, J. C. (2011). Upper-mantle seismic anisotropy from SKS splitting in the South American stable platform: A test of asthenospheric flow models beneath the lithosphere. *Lithosphere*, *3*(2), 173–180. https://doi.org/10.1130/L99.1

Babuška, V., Plomerová, J., & Vecsey, L. (2008). Mantle fabric of western Bohemian Massif (central Europe) constrained by 3D seismic *P* and *S* anisotropy. *Tectonophysics*, *462*(1), 149–163. https://doi.org/10.1016/j.tecto.2008.01.020

Babuška, V., Plomerová, J., & Šílený, J. (1993). Models of seismic anisotropy in the deep continental lithosphere. *Physics of the Earth and Planetary Interiors*, *78*(3), 167–191. https://doi.org/10.1016/0031-9201(93)90154-2

Barruol, G., Silver, P. G., & Vauchez, A. (1997). Seismic anisotropy in the eastern United States: Deep structure of a complex continental plate. *Journal of Geophysical Research*, *102*(B4), 8329–8348. https://doi.org/10.1029/96JB03800

Bastow, I. D., Thompson, Da, Wookey, J., Kendall, J. M., Helffrich, G., Snyder, D. B., et al. (2011). Precambrian plate tectonics: Seismic evidence from northern Hudson Bay, Canada. *Geology*, *39*(1), 91–94. https://doi.org/10.1130/G31396.1

Brun, J.-P. (2002). Deformation of the continental lithosphere: Insights from brittle-ductile models. *Geological Society, London, Special Publications*, *200*(1), 355–370. https://doi.org/10.1144/GSL.SP.2001.200.01.20

Deschamps, F., Lebedev, S., Meier, T., & Trampert, J. (2008). Stratified seismic anisotropy reveals past and present deformation beneath the east-central United States. *Earth and Planetary Science Letters*, *274*(3-4), 489–498. https://doi.org/10.1016/j.epsl.2008.07.058

Eakin, C. M., Obrebski, M., Allen, R. M., Boyarko, D. C., Brudzinski, M. R., & Porritt, R. (2010). Seismic anisotropy beneath Cascadia and the Mendocino triple junction: Interaction of the subducting slab with mantle flow. *Earth and Planetary Science Letters*, *297*(3), 627–632. https://doi.org/10.1016/j.epsl.2010.07.015

Fowler, C. M. B. (1990). *The solid Earth: An introduction to global geophysics*. Cambridge, UK: Cambridge University Press. Retrieved 2020-03-15, from https://linkinghub.elsevier.com/retrieve/pii/026481729390088A

Frederiksen, A. W., & Bostock, M. G. (2000). Modelling teleseismic waves in dipping anisotropic structures. *Geophysical Journal International*, *141*(2), 401–412. https://doi.org/10.1046/j.1365-246X.2000.00090.x

Frederiksen, A. W., Folsom, H., & Zandt, G. (2003). Neighbourhood inversion of teleseismic Ps conversions for anisotropy and layer dip. *Geophysical Journal International*, *155*(1), 200–212. https://doi.org/10.1046/j.1365-246X.2003.02043.x

Goldstein, P., & Snoke, A. (2005). SAC Availability for the IRIS Community. Incorporated Institutions for Seismology Data Management Center Electronic Newsletter.

Gueydan, Fdric, Morency, C., & Brun, J.-P. (2008). Continental rifting as a function of lithosphere mantle strength. *Tectonophysics*, *460*(1), 83–93. https://doi.org/10.1016/j.tecto.2008.08.012

Heit, B., Sodoudi, F., Yuan, X., Bianchi, M., & Kind, R. (2007). An *S* receiver function analysis of the lithospheric structure in South America. *Geophysical Research Letters*, *34*, L14307. https://doi.org/10.1029/2007GL030317

Lamarque, G., & Julià, J. (2019). Lithospheric and sublithospheric deformation under the Borborema Province of northeastern Brazil from receiver function harmonic stripping. *Solid Earth*, *10*(3), 893–905. https://doi.org/10.5194/se-10-893-2019

Latifi, K., Kaviani, A., Rümpker, G., Mahmoodabadi, M., Ghassemi, M. R., & Sadidkhouy, A. (2018). The effect of crustal anisotropy on SKS splitting analysis—Synthetic models and real-data observations. *Geophysical Journal International*, *213*(2), 1426–1447. https://doi.org/10.1093/gji/ggy053

Levin, V., Okaya, D., & Park, J. (2007). Shear wave birefringence in wedge-shaped anisotropic regions. *Geophysical Journal International*, *168*(1), 275–286. https://doi.org/10.1111/j.1365-246X.2006.03224.x

Licciardi, A., & Piana Agostinetti, N. (2016). A semi-automated method for the detection of seismic anisotropy at depth via receiver function analysis. *Geophysical Journal International*, *205*(3), 1589–1612. https://doi.org/10.1093/gji/ggw091

Liu, K. H. (2009). NA-SWS-1.1: A uniform database of teleseismic shear wave splitting measurements for North America. *Geochemistry, Geophysics, Geosystems*, *10*, Q05011. https://doi.org/10.1029/2009GC002440

Liu, S., Tommasi, A., Vauchez, A., & Mazzucchelli, M. (2019). Crust-mantle coupling during continental convergence and break-up: Constraints from peridotite xenoliths from the Borborema Province, northeast Brazil. *Tectonophysics*, *766*, 249–269. https://doi.org/10.1016/j.tecto.2019.05.017

Long, M. D., Benoit, M. H., Chapman, M. C., & King, S. D. (2010). Upper mantle anisotropy and transition zone thickness beneath southeastern North America and implications for mantle dynamics. *Geochemistry, Geophysics, Geosystems*, *11*, Q10012. https://doi.org/10.1029/2010GC003247

Mainprice, D., Barruol, G., & Ismaïl, W. B. (2000). The Seismic anisotropy of the Earth's mantle: From single crystal to polycrystal. In S.-I. Karato, A. Forte, R. Liebermann, G. Masters, & L. Stixrude (Eds.), *Earth's Deep Interior: Mineral Physics and Tomography From the Atomic Scale to the Global Scale*, *Geophysical Monograph Series* (pp. 117, pp. 237–264). American Geophysical Union. ISBN: 9780875909752.

Martin-Short, R., Allen, R. M., Bastow, I. D., Totten, E., & Richards, M. A. (2015). Mantle flow geometry from ridge to trench beneath the Gorda-Juan de Fuca plate system. *Nature Geoscience*, *8*(12), 965–968. https://doi.org/10.1038/ngeo2569

McNamara, D. E., Owens, T. J., Silver, P. G., & Wu, F. T. (1994). Shear wave anisotropy beneath the Tibetan Plateau. *Journal of Geophysical Research*, *99*(B7), 13,655–13,665. https://doi.org/10.1029/93JB03406

Meissner, R., Mooney, W. D., & Artemieva, I. (2002). Seismic anisotropy and mantle creep in younger orogens. *Geophysical Journal International*, *149*, 1–14.

Nicolas, A., & Christensen, N. I. (2013). Formation of anisotropy in upper mantle peridotites - A review. In K. Fuchs & C. Froidevaux (Eds.), *Composition, structure and dynamics of the lithosphere-asthenosphere system*. https://doi.org/10.1029/GD016p0111

Owens, T., & Wu, F. (1991). Tibetan Plateau Passive-Source Experiment. International Federation of Digital Seismograph Networks. Dataset/Seismic Network. 10.7914/SN/XC_1991.

Pandey, S., Yuan, X., Debayle, E., Tilmann, F., Priestley, K., & Li, X. (2015). Depth-variant azimuthal anisotropy in Tibet revealed by surface wave tomography. *Geophysical Research Letters*, *42*, 4326–4334. https://doi.org/10.1002/2015GL063921

Park, J., Yuan, H., & Levin, V. (2004). Subduction zone anisotropy beneath Corvallis, Oregon: A serpentinite skid mark of trench-parallel terrane migration? *Journal of Geophysical Research*, *109*, B10306. https://doi.org/10.1029/2003JB002718

Piana Agostinetti, N., & Miller, M. S. (2014). The fate of the downgoing oceanic plate: Insight from the northern Cascadia subduction zone. *Earth and Planetary Science Letters*, *408*, 237–251. https://doi.org/10.1016/j.epsl.2014.10.016

Plomerová, J., & Babuška, V. (2010). Long memory of mantle lithosphere fabric European LAB constrained from seismic anisotropy. *Lithos*, *120*(1), 131–143. https://doi.org/10.1016/j.lithos.2010.01.008

Plomerová, J., Šílený, J., & Babuška, V. (1996). Joint interpretation of upper-mantle anisotropy based on teleseismic *P*-travel time delays and inversion of shear-wave splitting parameters. *Physics of the Earth and Planetary Interiors*, *95*(3), 293–309. https://doi.org/10.1016/0031-9201(95)03122-7

Reiss, M. C., & Rümpker, G. (2017). SplitRacer: MATLAB code and GUI for semiautomated analysis and interpretation of teleseismic shear-Řwave splitting. *Seismological Research Letters*, *88*(2A), 392–409. https://doi.org/10.1785/0220160191

Romanowicz, B., & Yuan, H. (2012). On the interpretation of SKS splitting measurements in the presence of several layers of anisotropy: Interpretation of SKS splitting measurements. *Geophysical Journal International*, *188*(3), 1129–1140. https://doi.org/10.1111/j.1365-246X.2011.05301.x

Roth, J. B., Fouch, M. J., James, D. E., & Carlson, R. W. (2008). Three-dimensional seismic velocity structure of the northwestern United States. *Geophysical Research Letters*, *35*, L15304. https://doi.org/10.1029/2008GL034669

Rümpker, G., & Silver, P. G. (1998). Apparent shear-wave splitting parameters in the presence of vertically varying anisotropy. *Geophysical Journal International*, *135*(3), 790–800. https://doi.org/10.1046/j.1365-246X.1998.00660.x

Savage, M. K. (1999). Seismic anisotropy and mantle deformation: What have we learned from shear wave splitting? *Reviews of Geophysics*, *37*(1), 65–106. https://doi.org/10.1029/98RG02075

Sherrington, H. F., Zandt, G., & Frederiksen, A. (2004). Crustal fabric in the Tibetan Plateau based on waveform inversions for seismic anisotropy parameters. *Journal of Geophysical Research*, *109*, B02312. https://doi.org/10.1029/2002JB002345

Silver, P. G., & Chan, W. W. (1991). Shear wave splitting and sub continental mantle deformation. *Journal of Geophysical Research*, *96*(B10), 16,429–16,454.

Silver, P., Mainprice, D., Ben-Ismail, W., Tommasi, A., & Barruol, G. (1999). Mantle structural geology from seismic anisotropy.
Silver, P. G., & Savage, M. K. (1994). The interpretation of shear-wave splitting parameters in the presence of two anisotropic layers. *Geophysical Journal International*, *119*(3), 949–963. https://doi.org/10.1111/j.1365-246X.1994.tb04027.x
Vauchez, A., Tommasi, A., & Barruol, G. (1998). Rheological heterogeneity, mechanical anisotropy and deformation of the continental lithosphere. *Tectonophysics*, *296*(1-2), 61–86. https://doi.org/10.1016/S0040-1951(98)00137-1
Vecsey, L., Plomerová, J., & Babuška, V. (2008). Shear-wave splitting measurements—Problems and solutions. *Tectonophysics*, *462*(1), 178–196. https://doi.org/10.1016/j.tecto.2008.01.021
Vergne, J., Wittlinger, G., Farra, V., & Su, H. (2003). Evidence for upper crustal anisotropy in the Songpan-Ganze (northeastern Tibet) terrane. *Geophysical Research Letters*, *30*(11), 1552. https://doi.org/10.1029/2002GL016847
Wessel, P., Smith, W. H. F., Scharroo, R., Luis, J., & Wobbe, F. (2013). Generic mapping tools: Improved version released. *Eos, Transactions American Geophysical Union*, *94*(45), 409–410. https://doi.org/10.1002/2013EO450001
Yang, B. B., Liu, Y., Dahm, H., Liu, K. H., & Gao, S. S. (2017). Seismic azimuthal anisotropy beneath the eastern United States and its geodynamic implications. *Geophysical Research Letters*, *44*, 2670–2678. https://doi.org/10.1002/2016GL071227
Yuan, H., & Levin, V. (2014). Stratified seismic anisotropy and the lithosphere-asthenosphere boundary beneath eastern North America. *Journal of Geophysical Research: Solid Earth*, *119*, 3096–3114. https://doi.org/10.1002/2013JB010785